TAMPEREEN TEKNILLINEN YLIOPISTO
TAMPERE UNIVERSITY OF TECHNOLOGY

Jiawei Li

Nanofabrication by three-dimensional lithography

Master of Science Thesis

Examiner: Associate Prof. Tapio Niemi
Examiner and topic approved by the Faculty Council of the Faculty of Natural Sciences on 3 June 2015

ABSTRACT

Jiawei Li: Nanofabrication by three-dimensional lithography
TAMPERE UNIVERSITY OF TECHNOLOGY
Master of Science Thesis, 37 pages, 5 Appendix pages
May 2015
Master's Degree Programme in Science and Bioengineering
Major: Nanotechnology
Examiner: Associate Professor Tapio Niemi

Keywords: Nanofabrication, 3D lithography, Two-photo polymerization

Accompanied with the rapid improvement of technology, creating three-dimensional micro- and nanostructures has become much more important to satisfy various demands. However, conventional techniques are usually used for planar structures which are not suitable to generate true three-dimensional structures. Three-dimensional direct laser writing, as an advanced micro- and nanofabrication technique, provides the way to produce arbitrary micro- and nanostructures. Therefore, in this thesis, we employ 3D lithography to fabricate the three-dimensional structure. In addition, further research using the achieved structure to form colloidal crystal will be briefly introduced.

PREFACE

The work presented in this thesis has been done at the Nanoscience Center in the University of Jyväskylä from May 2014 to November 2014.

Firstly, I would like to thank Professor Ilari Maasilta for providing me the opportunity to work on this interesting topic in Jyväskylä and also for his guidance and ideas during the research. Moreover, I would like to thank Mr. Geng Zhuoran for guiding me the experimental instruments and Ms. Tian Yaolan for her advices and help with the research. I would also like to express my sincere gratefulness to NanoScience Center (NSC) for allowing me to use their cleanroom facilities.

In addition, I would like to thank Associate Professor Tapio Niemi and Dr. Janne Simonen for their encouragement and support during my master's study.

Tampere, 28.7.2015

Jiawei Li

CONTENTS

LIST OF SYMBOLS AND ABBREVIATIONS

3D Three dimensional

DLW Direct laser writing

UV Ultraviolet

Voxel Volume element

TPP Two-photon polymerization

TPA Two-photon absorption

1PA Single-photon absorption

PS Polystyrene

PMMA Poly(methyl-methacrylate)

TPE Two-photon excitation

PGMEA Propylene glycol monomethyl ether acetate

CF_4 Carbon tetrafluoride

CHF_3 Trifluoromethane

KOH Potassium hydroxide

UHV Ultra high vacuum

SEM Scanning electron microscope

Au Gold

As_2S_3 Arsenic Trisulfide

1 INTRODUCTION

Lithography, a method used to manufacture the components of semiconductor devices, has drawn great attention in the fabrication of micro- and nanostructures during last decades. [1,2] The word lithography comes out on the basis of two Greek words, Lithos and Grapheins, and it relates to a phenomenon that was invented by Alois Senefelder in 1798. [3] After that, the development of this technique contributes to enormous progress in many kinds of fields. However, with the trend towards miniaturization and complexity of devices, fabricating three-dimensional micro- and nanostructures has become much more desirable in order to fulfill diverse requisites. [4] Some lithographic techniques, such as electron beam and optical lithography, are essentially planar techniques which are limited to producing two-dimensional (2D) structures. There is no doubt that it will require a great deal of experimental work to build up 3D structures by these techniques. [5] Some other common 3D prototyping techniques, like 3D inject printing and UV laser stereo-lithography [6], have the capability to generate those 3D structures as well. Nevertheless, the maximum resolution of the obtained structures can be only a few micrometers. [6] For these reasons, we apply three-dimensional lithography to produce the 3D structures.

3D lithography is an innovative technology which is based on two-photon polymerization (TPP) effect. It plays currently a key role in manufacturing three-dimensional microstructures. It has been a used tool for many microfabrication research studies over the world. [4,7] A large quantity of advantages by making use of this technique have been manifested. One of the important strengths is that it can fabricate true 3D structures that can achieve sub-100 nm resolution beyond the diffraction limit. [6] Furthermore, it offers a faster way to create structures that are even more complex or maybe impossible for conventional lithographic techniques. Additionally, the achieved structures have a large number of applications, for example, in micro-electro-mechanical system (MEMS), photonics, biological etc. [8-10]

The target of this research is to generate a large, stable and smooth hollow box with the 3D lithography technique. Then based on the obtained structure, a further study can be carried out where polystyrene (PS) nanospheres will be self-assembled into crystals in the box, which ultimately will be utilized to test thermal properties by growing some

wires on the crystal. In this study, we mainly focus on the procedures of fabricating the 3D structure. In addition, several further experiments by dipping the attained box structure with a nanospheres solution will also be discussed briefly.

In this thesis, Chapter 2 will outline the theory and principles of 3D lithography. Moreover, it will also describe the research that has been done previously. Chapter 3 introduces the primary instrument used in this research. The experimental work will be present in Chapter 4. Chapter 5 will discuss the results and existing problems in the study. Chapter 6 gives the conclusion about the research.

2 THEORY AND BACKGROUND

2.1 Two-photon Polymerization

Two-photon polymerization (TPP) is a serial process which combines two-photon absorption and subsequently polymerization. It was defined as a tool for the fabrication of 3D structures in 1997, a paper published by Kawata and coworkers. [11] From then, the research on TPP has grown rapidly making it a fairly incomparable technique. [6,11]

Nowadays, TPP has already become a functional tool in plenty of areas, such as micro/nanophotonics, microelectronics, bioengineering, microfluidics and so on. [11] Undoubtedly, as one of the most prospective technologies for manufacturing three-dimensional micro-structures, TPP shows many remarkable characteristics. [12-14] For instance, it has the ability to produce small structures with superior resolution and without topological constrains. [13] It can eliminate the influence that maybe caused by the humidity variation from the surrounding environment, because the polymerization process happens inside the photopolymer. Apart from these, the operation condition of this procedure is very simple, as it does not require any mask, mold or stamp. [14] What's more, any kind of 3D structures based on computer generated models can be obtained by this method. [13]

2.1.1 Two-photon absorption

Two-photon absorption (TPA) was first predicted in 1931 by Maria Göppert-Mayer in her doctoral thesis. [15] It is a non-linear optical (NLO) phenomenon that takes place when a molecular transition is induced from the ground state to a higher electronic state in a single step -- with two photons absorbed simultaneously. [16] When the energy of each photon is the same, the process is said to be degenerate, otherwise, it is called nondegenerate. Most of the applications use the degenerate technique because of the simplicity of the experimental setup. *Figure 1* shows an example of degenerate two-photon absorption. [11,17]

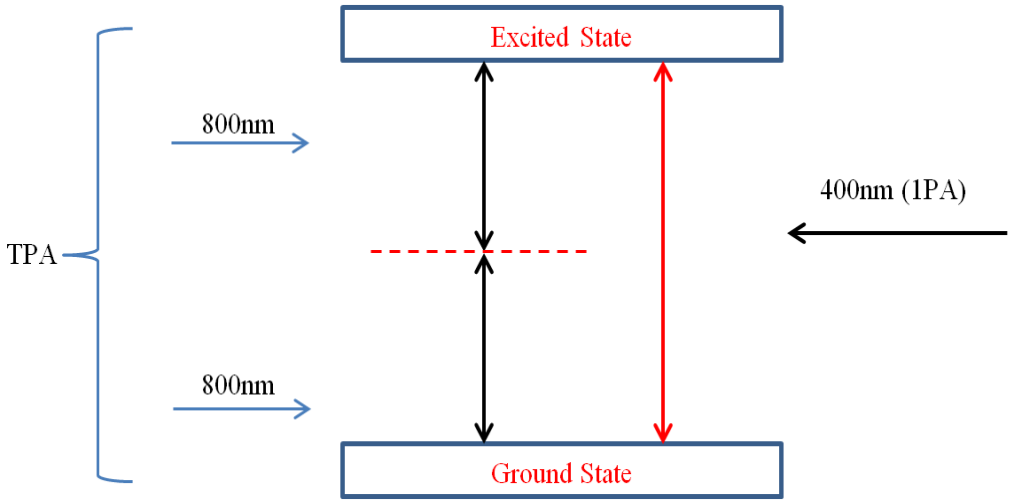

Figure 1. *Scheme of TPA process. [17]*

In general, TPA is a very useful tool in laser spectroscopy since the selection rule for two-photon excitation (TPE) is different from that of single-photon absorption. [18] TPA makes it possible to observe the transitions between two states that cannot be connected to atomic ground level by electric-dipole transition. [16] Practically, there are two types of electron excitations for absorbance of two-photon energy: simultaneously and stepwise. Different from simultaneous TPA, stepwise relies on a real intermediate energy, while simultaneous TPA occurs via a virtual energy level, as illustrated in *Figure 2*. Stepwise TPA can also be considered as two sequential single-photon absorptions, which does not require coherence of the incident light. [19] In this research, however, we only concentrate on simultaneous TPA.

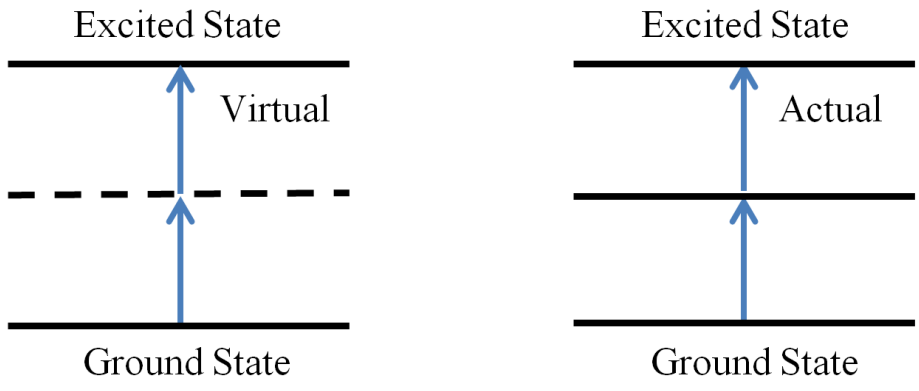

Figure 2. *Illustration of two-photon absorption scheme. (a) simultaneous TPA, and (b) stepwise TPA. [19]*

As a primary non-linear effect, TPA is closely related to Raman scattering because both are two-photon processes. [13,16] While spontaneous Raman scattering was observed in

1928, the experimental results of TPA were not first observed until 1961 by Kaiser and Garrett, after the first working laser. [18,20] The main reason for the difference is that in Raman scattering process only one photon is absorbed and the other is simultaneously emitted. Therefore, for Raman scattering, the scattered light intensity is proportional to the intensity of the incident light whereas in TPA the absorption probability is small but proportional to the square of the intensity of incoming light. As a result, in order to observe TPA, the intensity of the incident laser light has to be high enough. [13,17]

For two-photon absorption, one of the advantages is that the effect of elastic scattering can be decreased drastically during the process. The relationship between scattering and wavelength can be described according to the Rayleigh's law, which states:

$$\sigma_s = \alpha \frac{1}{\lambda^4} \qquad [17]$$

where σ_s is the scattering cross section of the molecule and λ is the wavelength. As we can see from the equation, when the wavelength of light becomes twice the absorption wavelength of materials, the scattering of light is reduced by 16 times. This property also gives the chance to increase the penetration depth inside the material and reduce the size of the focal spot. [17,21]

In addition, the cross-section of TPA, δ, is typically used to describe the non-linear optical properties of molecules. The attenuation of the light beam resulting from TPA can be calculated following the equation below:

$$\frac{\partial I}{\partial z} = -\beta I^2 = -N\delta FI \qquad [22]$$

where I is the intensity, z is distance into the medium, β is the molecular coefficient of TPA, N is the number of molecules per unit volume and F is the photon flux. [22] Essentially, the cross-section of TPA that quoted in the units of Göppert-Mayer (GM) is much lower than that of one-photon absorption, usually on the order of 1 GM or less, where 1 GM equals to $10^{-50}\ cm^4 secphoto^{-1}$. As a result, to promote two-photon absorption, high local photon fluxes will be needed. [11] This property is one of the reasons that contribute to getting low background noise and better resolution by this method. [17] All these properties help TPA to have a wide range of applications.

2.1.2 Photopolymerization

Photopolymerization is a process that can be induced by (two-) photon absorption. We can define this phenomenon as a chemical reaction that utilizes light as the reaction trigger to create macromolecules. Photopolymerization is also one of the most

prominent methods applied to create 3D structures. One of the important benefits of this method is that the photopolymerized structures can have real physical shape. This is according to the phenomenon that the resins will harden after laser irradiation by undergoing a phase transition from liquid to solid. Afterwards, non-polymerized liquid will be easily removed in the developing bath and solidified 3D structures are attained. [19,22,23]

Polymerization by two-photon absorption also includes some other benefits. For example, the excitation beam employed in one-photon absorption polymerization process is normally a conventional source so that linear absorption will happen during that process. As a consequence, it will lead to the excitation attenuating dramatically before the beam reaches the focal point which finally causes only the top layer of photoresist to be polymerized. When the intensity of the laser is increased, it may result the polymerization of all the material along the optical axis, or boiling away of the material, if the energy dumped into the system is too high. Thus, it is not possible to fabricate 3D microstructures due to lack of polymerization control using one-photon absorption. In contrast, polymerization can be restricted to a small volume around the focal point after two-photon absorption. [11] Then, any arbitrary 3D structures can be manufactured by either scanning the laser beam through the resin volume or by moving the sample in three dimensions. [22]

Usually, photopolymerization process comes up via several steps: initiation, propagation and termination. [23] The diagram of this chemical reaction process is shown in *Figure 3*, where I represents photoinitiator, I* is the intermediate state of the photoinitiator, R* represents free radicals, M represents monomers or oligomers, M* represents propagating radical.

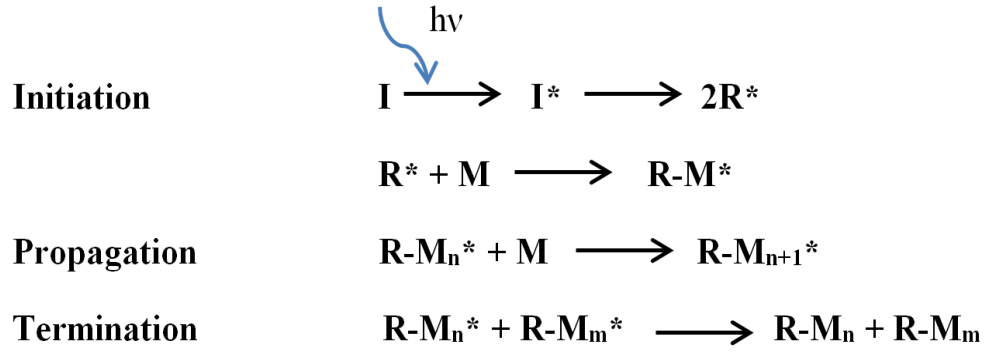

Figure 3. *Basic scheme of radical polymerization. [23]*

The initiation step includes two reactions. The first one is the dissociation of initiator molecule I to form the free radicals R* by absorbing light photons. The second reaction

of initiation is to produce chain-initiating radical R-M* through the reacting between radicals and the first monomer molecules M. The propagation step is creating new radicals successively through the additions of new monomers. Termination step happens relying on the combination reaction between chained radicals, which finally makes the process a chain reaction. [23,24]

2.2 Principle of 3D Direct Laser Writing

Three-dimensional direct laser writing (DLW), also known as 3D lithography, is a promising tool which offers means of producing three-dimensional structures. It can be recognized as 3D extension of planar electron-beam and optical lithography and allows for producing the 3D micro- or nanostructures directly inside the material (see *Figure 4*). In essence, in this technique, femtosecond pulsed laser light is tightly focused inside a photoresist but at a wavelength at which the photoresist is transparent. E-patterning occurs by taking advantage of the two-photon polymerization (TPP) effect that was described before. Using TPP, the chemical and physical properties of the photoresist are altered within a small volume that is restricted by the irradiated laser intensity. Generally, this volume pixel is called "voxel" and is commonly in the shape of ellipsoid, allowing fabrication of 2D and 3D structures with high resolution and arbitrary shapes. [8,25] The unexposed parts of the photoresist will be washed away in the developer bath. Finally, a free-standing three-dimensional structure is achieved. [25]

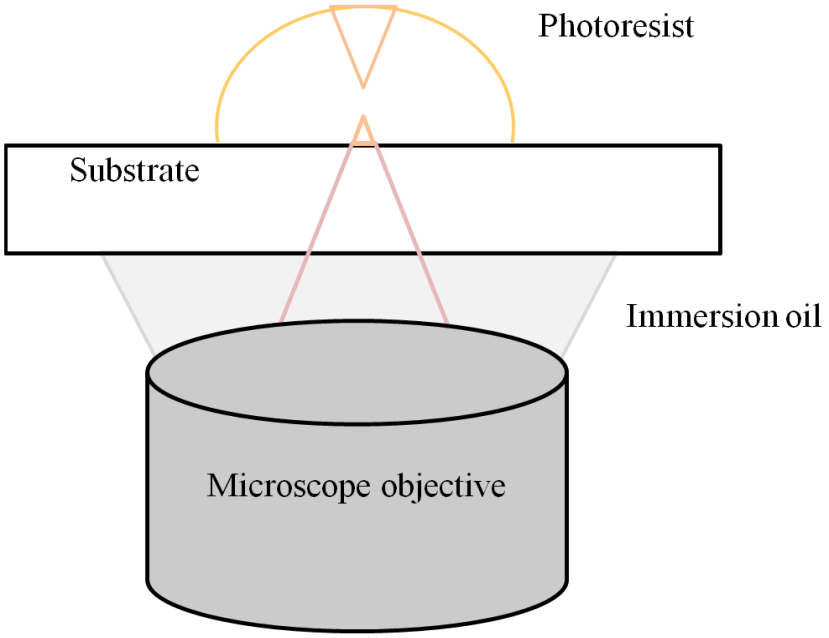

Figure 4. *Scheme of regular three-dimensional direct-laser writing optical lithography. [26]*

2.3 Previous research

As mentioned in the beginning, the aim of the research is to apply the three-dimensional lithography technique to manufacture a hollow structure which can be employed for self-assembly of lattices of nanoparticles. [27] The figure of the entire square shaped structure is shown in *Figure 5*.

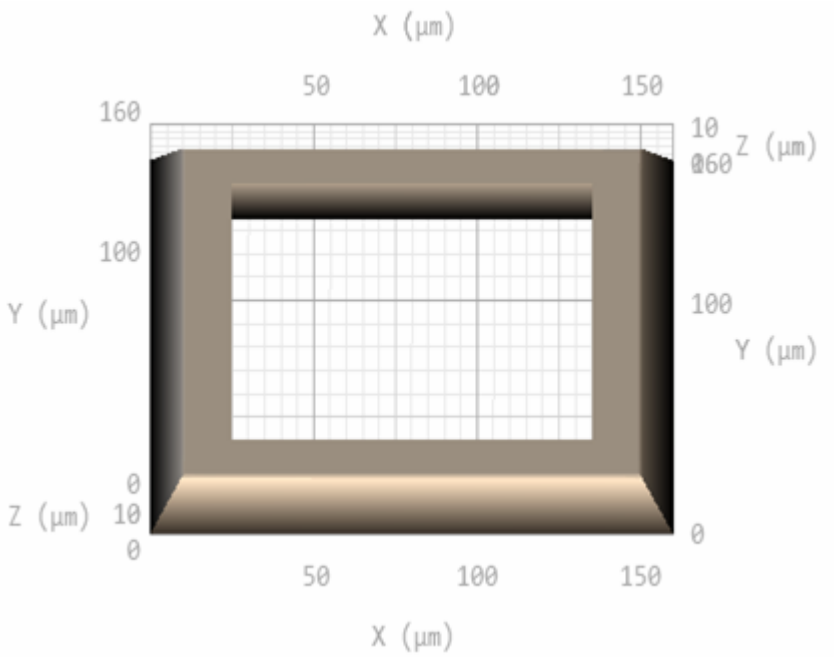

Figure 5. *A scheme of the total structure, with the length of the outer side 160 µm, and inner side 100 µm. The width of the sloped regions and the height of the whole frame is 10 µm.*

Before utilizing the technology in this work, several other researches had already been done previously. One of them was making use of a two-step e-beam lithography technique to produce a 3D structure by etching into Si substrates by the processes shown in *Figure 6*. [28]

In that research, some troughs were first fabricated into silicon substrates with dimensions of $8\,mm \times 16\,mm$. During this procedure, Poly(methyl_methacrylate) (PMMA) was chosen as the resist and the overlay SiN_x layer (750 nm) was used as the Si etch mask. The nitride mask was established by etching it in CF_4 or CHF_3 plasma. The troughs with the depth ranging from a few micrometers up to approximately 100 µm were formed by wet chemical etching in potassium hydroxide (KOH) at 90 ˚C, leading to a crystallographic sidewall angle of 54.74°. Afterwards, a second e-beam lithography process including lift-off alignment step was utilized to only coat the bottom of selective troughs with a hydrophilic TiO_x layer (nearly 10 nm thick). By dipping the

sample into the solution of PS nanospheres, multi-layer colloidal crystals were grown, as the nanospheres self-assembled from suspensions.

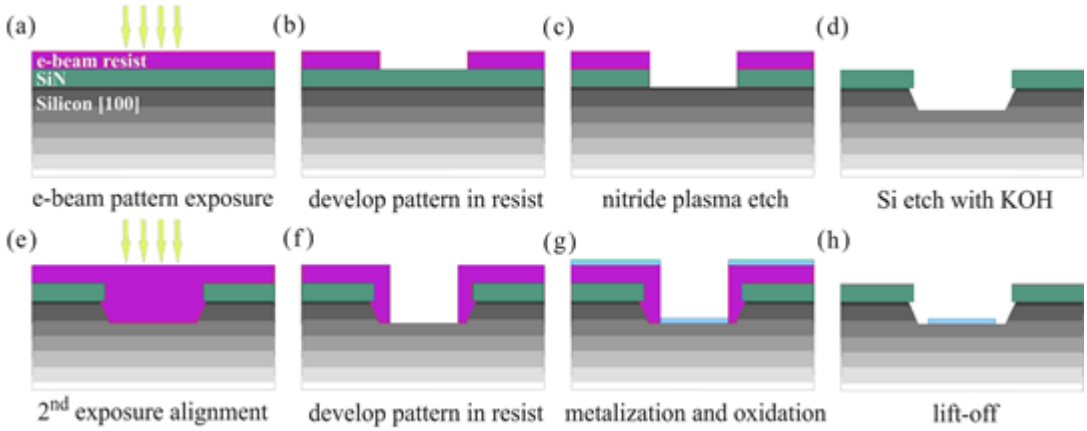

Figure 6. *Lithography process steps: (a) Pattern is exposed in e-beam resist (PMMA), (b) resist pattern is developed, (c) SiNx is etched with CF_4 plasma and then (d) the Si substrate is etched anisotropically with KOH. (e) Second lithography is aligned with the previous pattern, (f) pattern is developed, (g) UHV evaporation of Ti and oxidation followed by (h) final lift-off. [28]*

The results obtained from this technique indicated some benefits. Firstly, it reduced the cracks in multi-layer colloidal crystals, which were more of a problem for self-assembly without lithography. Furthermore, the size of the colloidal crystal domain could be as large as 200 µm, and the broad size distribution found in unaltered substrates was suppressed effectively. What's more, compared with other methods, this method was fast as large-scale colloidal crystal structures were produced in one step. *Figure 7* depicts an example of the results, where on the left a measurement image with the domains is showing, and on the right a thick multi-layer colloidal crystal structure is seen from the side-view. However, several problems still existed with this method. Some cracks still could develop, similar like plain self-assembled samples. In addition, although some formed crystal structures were free of cracks, they were not fully single crystalline. [28] Considering these problems, this study, it was decided to perform by using three-dimensional lithography to fabricate the hollow structure.

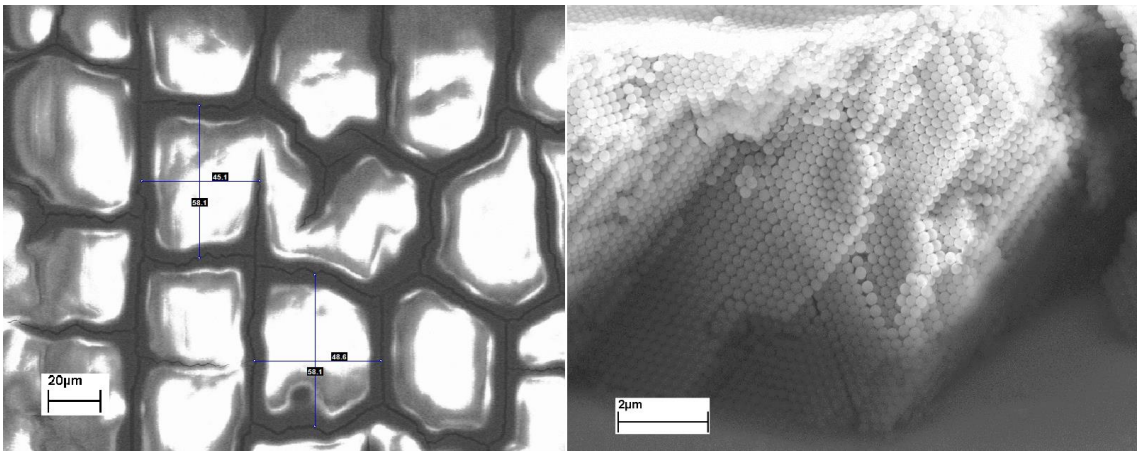

Figure 7. *An example of a SEM image used for the domain length measurements (left) with a side-view close up of the multi-layer colloidal crystal structure (right). Values shown for measured lengths are in µm. [28]*

However, some research by using the 3D lithography was also studied previously, in which the software Inventor was used to generate the structure in STereoLithography (STL) file (see *Figure 5*), which was converted to the 3D lithography instrument format (will be described in next chapter). The results achieved by this method exposed several problems. One of the significant problems was that the surfaces of slopes were not smooth enough but formed steps (see *Figure 8*). This would possibly prevent nanospheres and wires to climb on the slopes. Furthermore, this problem appeared in the conversion process which could not be eliminated. In addition, one small mistake during the slicing process would cause unnecessary extra lines occurring in the structure as seen in the middle part of the image below. Thus, here, we adopt another way to make the structure and then written it with 3D lithography.

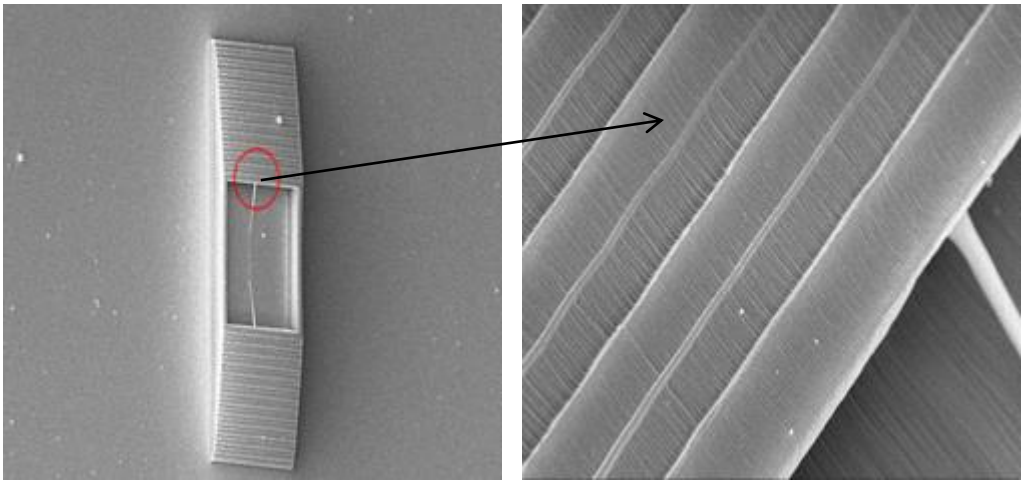

Figure 8. *An image example of the results with the structure formed by Inventor which was done by Ms. Tian Yaolan.*

3 EQUIPMENT

3.1 3D Direct Laser Writing setup

The instrument used in this research is a commercial two-photon DLW system (Photonic Professional *GT*) by Nanoscribe GmbH. *Figure 9* is a photograph of the 3D DLW system.

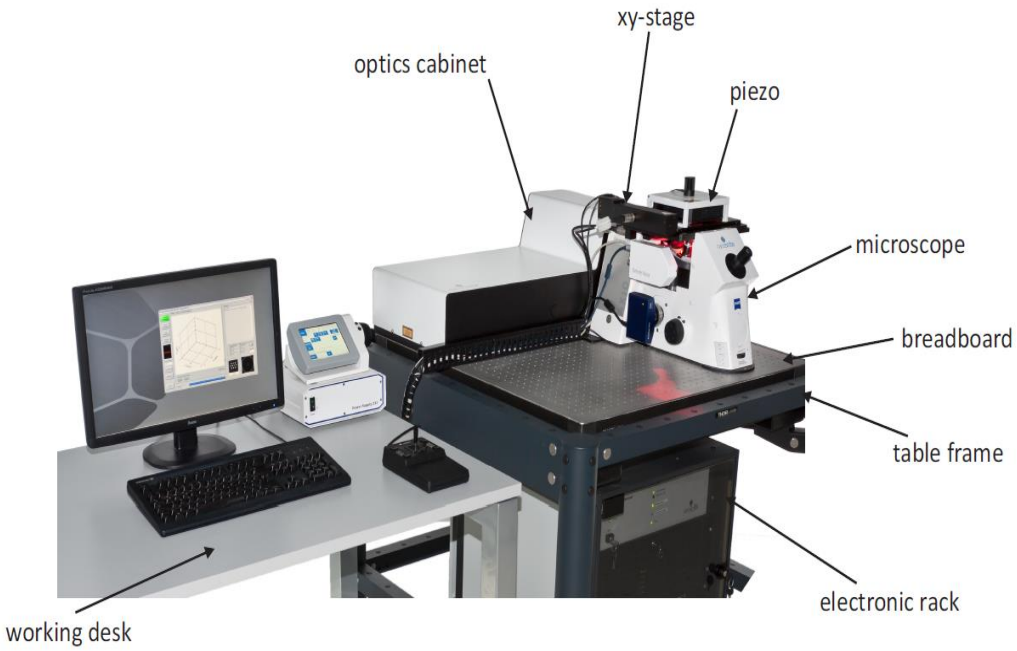

Figure 9. *Nanoscribe Photonic Professional system. [29]*

Essentially, in this system, a pulsed erbium doped femtosecond fiber laser is used with the center wavelength tuned to 780 nm. The pulse duration of the laser is around 100 fs, and the repetition rate is about 80 MHz. The femtosecond pulses will be focused to an objective with a high numerical aperture: NA=1.4. In addition, as displayed in *Figure 9*, the system is fixed on an optical breadboard which is passively vibration isolated from the table frame (a self-leveling system). The laser and the optics are assembled inside the optics cabinet. There is also a protective housing which is equipped with an electrical interlock switch screwed to the frame. Thus, when the housing is open, the

interlock switch is open, and the laser will be shut down. Moreover, a mechanical security shutter is installed in front of the laser emission aperture so that it can block the beam path when the housing is open. (There is one more electrical shutter which blocks the beam from going to the microscope when there is no exposure) The electrical rack under the optical table is employed to house the computer, laser controller, Nanoscribe controller and some other power supplies for the system components. [29, 30]

Other than these devices, the instrument also provides two ways for positioning: a xy-stage and a piezo stage. The piezo stage will be moved as a whole by any xy-stage movements since it is installed on top of the xy-stage. The xy-stage offers the opportunity to deal with different substrate chips and writing positions on one single substrate. During this research, we used only the piezo stage. Hence, the sample was put on a particular substrate holder on the three-axis piezo scanning stage with the scanning range is 300 μm^3.

The microscope consists of several different parts (see *Figure 10*). It can be operated by a docking station as shown in *Figure 11 (left)*, where all the relevant parameters can be set and adjusted. In addition, it includes two illuminations: transmission and reflection, which can be adjusted by the LED driver (see *Figure 11 (right)*). In this research, we only use the transmission illumination.

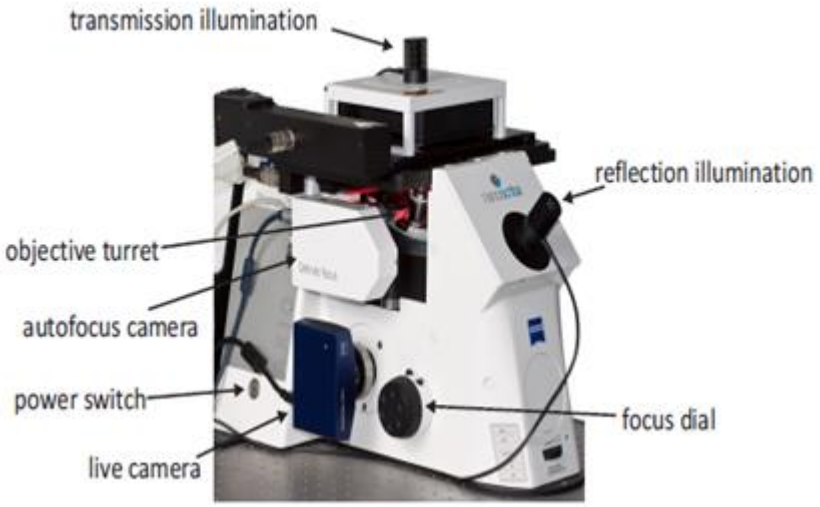

Figure 10. *Microscope with major components. [29]*

Figure 11. *Microscope docking station (left) and LED driver for transmission and reflection illumination (right). [29]*

The microscope system also contains an inverse microscope which has an autofocus system that is capable to focus the laser spot at the substrate surface automatically.

Except for the hardware mention above, Photonic Professional system also includes several specific software components. One of them is called NanoWrite, which encompasses some features so that the system could be calibrated and controlled manually. It also has the ability to monitor the direct laser writing process by including a camera that shows the live view. Therefore, a certain input file will be demanded for this software. In this system, the file format is called General Writing Language (GWL). Although the .gwl file can be edited by any text editor, a text editor Describe is recommended for this software. A .gwl file can not only describe the trajectories during the writing process but also set up the system parameters utilized in that process. Photonic professional system provides another software, Nanoslicer, to produce .gwl files via conversion from an exported STL file which can be exported by almost any modern computer-aided design (CAD) software. [29] However, in this study we use our own codes to produce the .gwl file in order to have ultimate control.

3.2 Photoresist

It is known that there are lots of photoresists which are available for the 3D lithography technique. [25] For example, the common negative-tone resist, SU-8, has been used for many different kinds of applications in the area of microfabrication. In addition, another negative-tone photoresist based on arsenic trisulfide (As_2S_3) provided by Nanoscribe also have been utilized for fabricating manifold structures such as 3D photonic crystals, resonators, photonic waveguides and so on. [25] However, here, a series of negative-

tone IP-photoresists which satisfied the requirements of this research are used. A lot of merits have been presented by using these photoresists. First and foremost, they can provide high resolution and high mechanical stability for structures in the micro- and sub-micron range. Secondly, these photoresists can be adhered quite well on glass substrates and are easy to manipulate. Additionally, these resists have typically low stress, little shrinkage and low proximity effect. *Table 1* shows some features of these IP-photoresists. In this study, we only use IP-L 780. [31]

Table 1. *Some features of IP-photoresists. [31]*

Features	IP-L (780)	IP-G (780)	IP-Dip
Refractive index at 780nm unexposed	1.48	~ 1.50	1.52
Prebake	No	Yes	No
Cast process	Drop casting	Drop casting or spin coating	Drop casting
Exposure	780nm for 2PP	780nm for 2PP	780nm for 2PP
Post bake	No	No	No
Developer	PGMEA/IPA	PGMEA/IPA	PGMEA/IPA

3.3 Applications

As a well-established technology, 3D DLW technology has already become a leader for three-dimensional micro- and nanofabrication. And based on its unique characteristics, it has been utilized in a number of different areas. Here, we list the prominent areas of this technology and several images, as seen in *Figure 12* which show the versatility of this 3D lithography.

Photonics: metamaterial, photonic crystals, distributed feedback lasers, photonic ring resonators, diffractive optics

Micro-optics: micro optical devices, integrated optics

Microfluidics: lab-on-a-chip system, development of substances

Life Sciences: cell migration, stem cell differentiation, tissue engineering

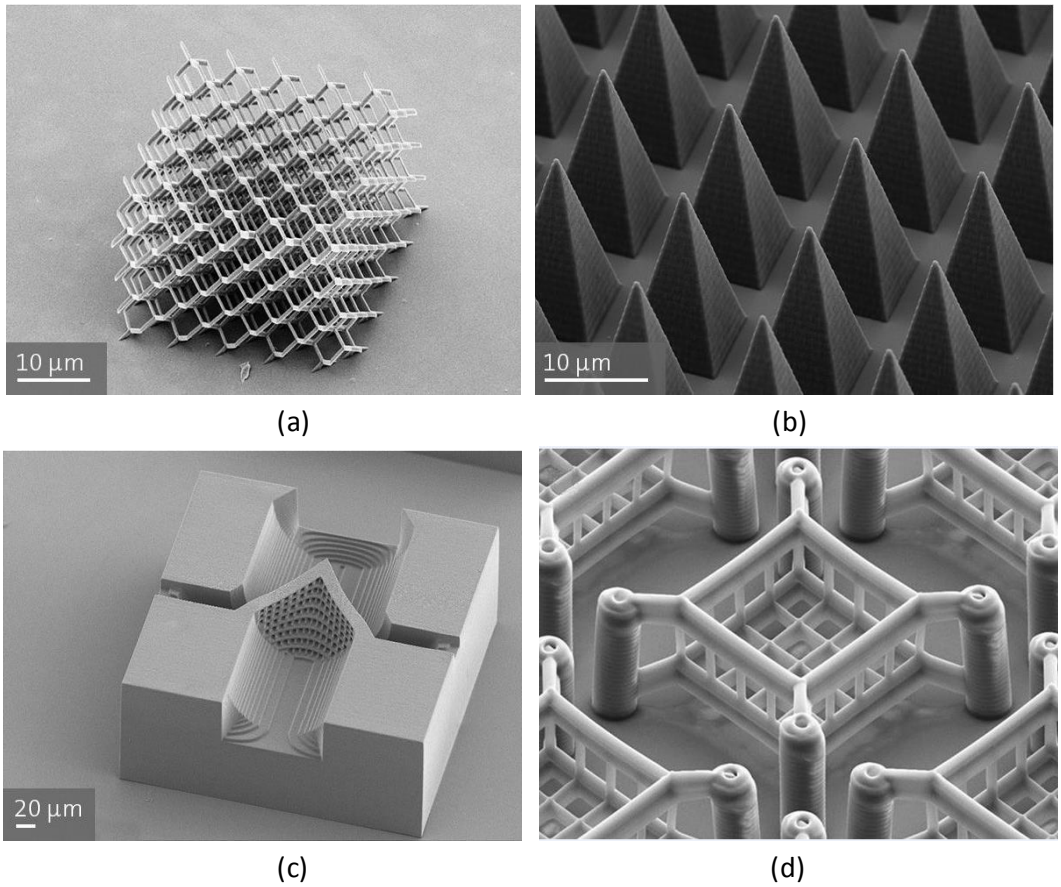

Figure 12. *(a) 3D photonic crystalline diamond (PCD) structure (the photoresist is IP-L 780); (b) Pyramid array for applications in micro-optics; (c) Microfluidic filter element structured in SU-8. Design by IMSAS; (d) SEM image of cell scaffolds. [32]*

Apart from these applications, at NSC, we are focusing on a new application: phononic crystals (PnCs). Phononic crystals are periodic structures with variation of elastic properties. Because of its special characteristic, phononic crystals will exhibit phononic band gaps that contribute to PnCs utilized in variety of areas, especially for thermal properties, such as thermal conductivity, thermo-electrics etc. [33] A possible way to form the 3D phononic crystals is by vertical self-assembly of PS nanospheres, in which a 3D structure is needed to be as the container. Therefore, here, the primary thing is to fabricate this 3D hollow box structure.

4 EXPERIMENTS

4.1 Optimization of writing parameters

Before we start fabricating the entire structure, it is necessary to establish the best suited parameters that are met this technique, since those factors will influence the whole procedure. One of the important factors is the value of laser power, which plays a quite significant role during the overall process. In addition, settling time, the amount of time the system waits between each line segment, is another key factor which can contribute to accelerating the process. Apart from these, the line distance in both x/y and z direction, as well as the writing speed are also essential factors and helpful in reducing the total fabrication time. [34]

Laser power: The laser power can be adjusted easily in 3D lithography. The exact parameters for the optimal laser power depend on the properties of the piezo scanner and the photosensitive resist material utilized, and can be controllable via two commands in the gwl-file. As a result, the actual laser power is defined as LaserPower*PowerScaling. When the PowerScaling is set on the default value 1 and the maximum LawerPower value is set at 100, then the system is set to around 20 mW power at the aperture of the objective. [29] In our research, a laser power of 40 % (8 mW) was utilized throughout the experiment.

Settling Time: The settling time is the length of time the system pauses after a line segment is drawn and before the next is started. The total structure consists of many lines, thus, the system will spend a lot of time waiting instead of writing. [29] Hence, although the default value of the settling time is 300 milliseconds, here, we set the value to 200 ms in the tests.

Line distance x/y: The line distance x/y is used to decide the distance between two neighboring lines in x- and y-direction. The maximum line distance depends on the voxel width, d_{xy}. In general, by increasing the line distance the overall number of lines can be reduced. A smaller line distance can lead to a more stable structure but will increase the writing time. [34]

Z distance, layer distance: Similar to the line distance, z distance is the distance between two neighboring individual layers of the structure that depends on the voxel length, d_z. The z distance has an effect on the overlapping parts between two layers which influence the stability of the structure. [29,34]

Writing speed: For this instrument, the writing speed can be calculated as follows: $\text{writing speed} = \text{update rate} \times \text{point distance}$, where update rate is the frequency that stage moves from point to point. However, in this research, as the structures are mainly composed by straight lines, a desired configuration is used which can dynamically adapt the writing speed to the trajectory based on the laser power and settling time we set.

The resolution in 3D lithography is mainly affected by the voxel size. Therefore, it is essential to make sure what size and shape of the voxel is in the beginning. [26] However, it is a considerable challenge to determine the voxel dimensions accurately. Several parameters, such as the laser power, the exposure time, the N.A. of the objective lens, the substrate etc. affect the shape and size of the voxel. In addition, a difficult problem is the truncation effect, which means that when voxels are written in the resist on the substrate, part of the voxel can be embedded in the substrate, leading to a partial voxel shape (see *Figure 13*). [21,35] On the other hand, if the voxels are fabricated above the substrate, they may be washed away during the developing process, if the developed voxel area is not connected to the substrate. [21] This problem is also complicated by the fact that the formed voxels cannot be viewed during the fabrication process but have to be imaged later. [35] Luckily, in reference [36] a solution was proposed to solve this problem, by employing an ascending scan exposure method. In this technique, a series of identical voxels are made at different heights relative to the surface of the substrate as we can see in *Figure 13*. At first, the voxels are embedded in the substrate. Then in the intermediate range, the formed voxels are just connected to the substrate and will remain there after developing, and can give a clear image of voxel dimensions. Finally, their dimensions can be evaluated quantitatively by observing the precise shape of these freestanding voxels with scanning electron microscopy. [21,35]

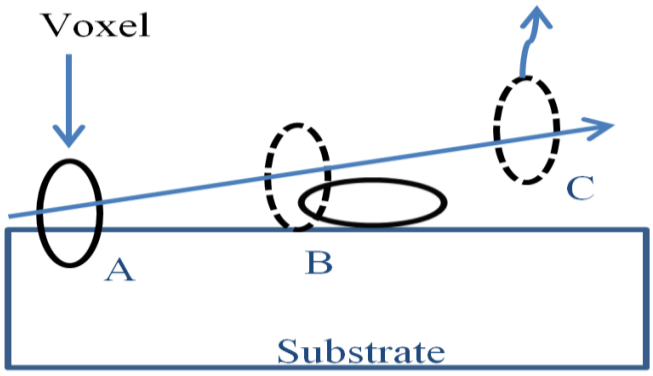

Figure 13. *The scheme of ascending scan exposure method: Voxels polymerized under different focusing height levels: A, an erected voxel; B, an overturned voxel; C, a floated voxel. [21]*

Figure 14 (a) illustrates a SEM image of some voxels in our tests with varying laser power, exposure time and the height relative to the substrate surface by using this ascending method. Here, IP-L 780 is chosen as the resist and a commercial glass is used as the substrate. For the whole tests, the laser power changes from 4 mW to 16 mW with an interval 2 mW, and the height relative to the substrate surface changes along y direction from 0 to 1 μm with an interval 0.1 μm, while the exposure time is just set at four different values: 1 ms, 10 ms, 100 ms, 1000 ms (from left to right) for different laser power. It is apparent as usual that the shape of the voxel is ellipsoidal, stretched in the z direction. And it shows the voxels will not be formed when the laser power and the exposure time values are very small (e.g. in the condition (6 mW, 1 ms)), however, when the values are quite big, the voxels will be burned. [21] *Figures 14 (b) and (c)* show two clearer images of voxels with different parameters.

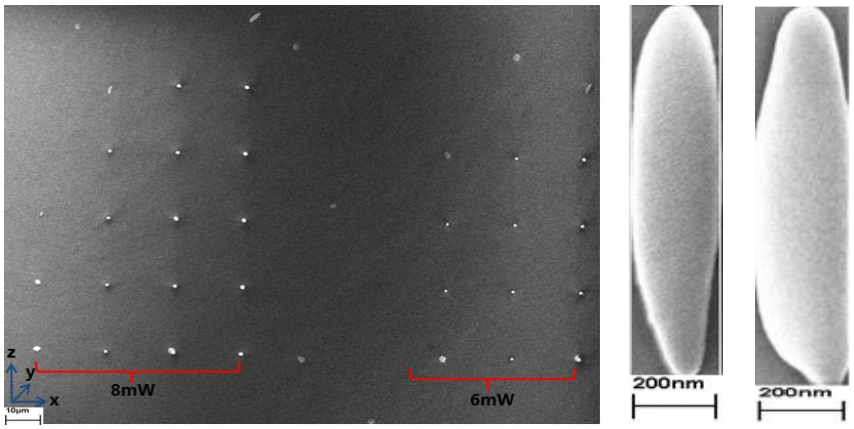

Figure 14. *(a) An top view of some voxels drawn by the ascending method; (b) A SEM image of one voxel obtained under (10 mW, 10 ms). The length for the voxel is around 1550 nm, the width is about 360 nm; (c) Another example produced by changing the exposure time (10 mW, 100 ms). The measured length is around 1880 nm and the width*

is about 400 nm.

From analysis of a large number of tests, some people have derived equations to calculate the voxel for NA>0.7: [34]

$$r_{xy} = \frac{0.325\lambda}{\sqrt{2}NA^{0.91}} \qquad r_z = \frac{0.532\lambda}{\sqrt{2}}\left[\frac{1}{n-\sqrt{n^2-NA^2}}\right] \qquad (1)$$

where λ is the wavelength of the laser, n is the refractive index of the medium and NA is the numerical aperture of the objective. Some information can be attained from these theoretical results. For example, by inserting the parameters from our system, λ=780 nm, NA=1.4, n=1.48, we get the voxel diameters: $d_{xy} = 2r_{xy} \approx 262$ nm and $d_z = 2r_z \approx 596$ nm. This can be compared with the usual diffraction limited resolution for a 780 nm light source with, $r_{xy}=0.61\lambda/NA \approx 340$ nm, showing that the two-photon resolution can be well below the usual diffraction limit. [34] Equations (1) also show that the NA is a quite important parameter for achieving minimum feature size, affecting the resolution in a nonlinear manner. According to these equations, the varieties of voxel sizes and the aspect ratio by changing the values of NA can be obtained, as depicted in *Figure 15*. Although the calculated aspect ratio of the voxel here is less than 3, in actual experiments, the aspect ratio is a little larger than it. In addition, an increase of the laser power or exposure time will increase the polymerized volume, and both of these can have an effect on the values of aspect ratio, as shown in *Figure 16*, but the specific relationships among them have not been understood completely. [34] This is not taken into account in Equations (1).

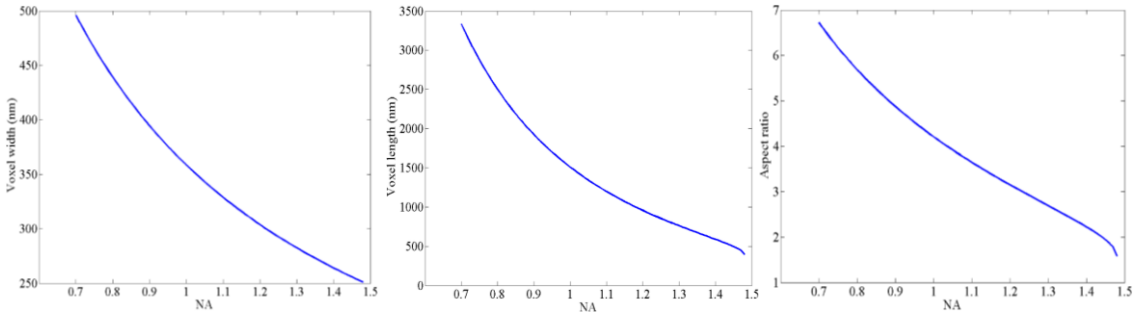

(a) (b) (c)

Figure 15. *Theoretical plots according to equations (1) with the same x axis (NA) but different y axis: (a) Voxel width; (b) Voxel length; (c) Aspect ratio.*

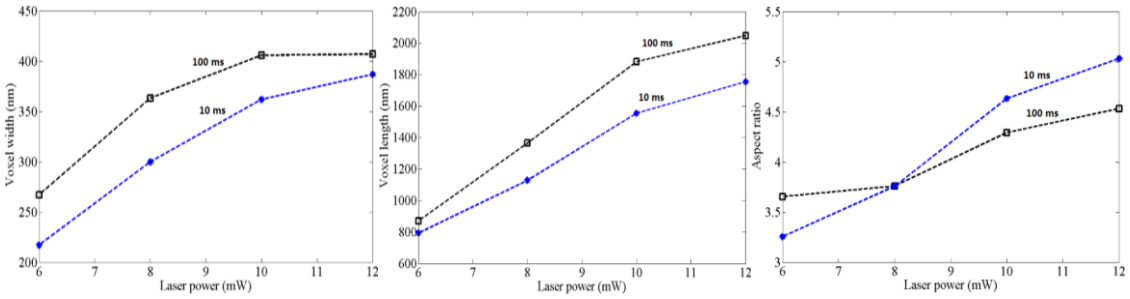

Figure 16. *Laser power-dependent experimental voxel dimensions and the aspect ratio under two different exposure time (10 ms and 100 ms).*

For our research, an approximate value 140 nm for the minimum voxel width is provided by the company. And as mentioned above, an automatic configuration is used which adjusts the scanning speed to a desired value at around 300 μm/s. Therefore, except the values of laser power and settling time, we only give the values of line distance x/y which is set at 100 μm and the z distance 200 μm for the 3D structure writing.

4.2 3D structure tests

After adjusting all the parameters used in the experiments, we started to fabricate the 3D structures. In this study, a commercial circular glass plate was used as the substrate with the diameter 30 mm and thickness 170 μm. The glass was first cleaned by acetone and isopropanol and then dried with nitrogen gas. Then, it was adhered to the sample holder with a droplet of Zeiss immersion oil on the bottom side of the substrate, and a droplet of IP-L 780 resist on the top side. The programming of the structure was done with Mathworks Matlab R2010b which has the function to store the formed file into gwl-format. [38] All the parameters, such as the laser power, the settling time etc., were edited with the text editor Describe (an example shown in the Appendix). [8] After these procedures, we could fabricate the structures by operating NanoScribe. Since the piezo stage will be moved precisely by the pre-programmed path, only part of the resist is exposed and polymerized. Hence, a free standing structure could be obtained after washing away the unexposed parts, by developing the sample in PGMEA (Propylene glycol monomethyl ether acetate) for around 20 minutes. After writing, the samples were coated with a thin layer of Au (nearly 7 nm) by using an electron-beam evaporator. Finally, the written structure could be examined with a SEM.

There were several challenges during the 3D writing tests. First, the program of the structure was made up of line segments which were defined with a three column array for x-, y- and z-coordinates. Thus, there were many different ways for designing the 3D structure which caused some trouble to find the suitable shape of it. For instance, when

the whole frame was produced by many straight lines, as illustrated in *Figure 17*, the entire structure did not adhere to the substrate tightly. This phenomenon could be explained by the deformation effect that is caused by the shrinkage of the materials during the developing process. [39] However, if we decreased the density of lines to decrease the deformation, the structure would not be mechanically stable but would collapse. A great deal of time would be needed if we made the tests with an entire box structure. Considering this, we decided to first make tests with a smaller structure to get the appropriate structural composition.

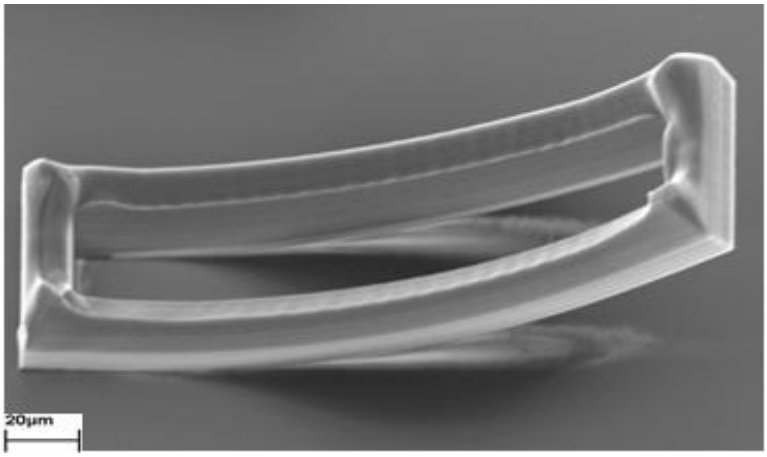

Figure 17. *An example of SEM image with the total structure fabricated with dense lines, forming a solid box.*

The smaller test structure was a small box with both of length and width 30 µm, and the height was 10 µm. The decision was made to use a hollow frame consisting of beams, to reduce deformation effects, shown in the *Figure 18*. In this frame, the distance between two horizontal lines was 5 µm (same as in the vertical direction), whereas along Z direction the spacing of the writing was set always at 200 nm producing a solid beam of height 10 µm in z-direction. In addition to these lines, some diagonal lines were also added to the structure to form triangular shapes. The reason for that was that the triangles kept the structure stable, and they were also straightforward to generate. Finally, all these beams were enclosed with an around 0.2 µm thick wall (formed by two layers) to hatch them together and to help to increase the stability of the structure as well. The distance between these two layers was 100 nm (an example of the Matlab code also shown in the Appendix).

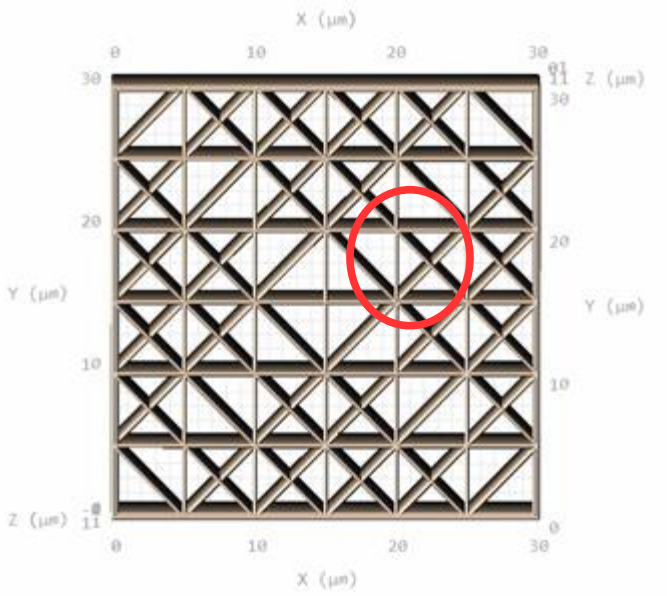

Figure 18. *The inner shape of small test structure (top view).*

Since the overall structure needs to be enclosed, we also added two layers on the top with the distance between two neighboring lines in lateral direction set at 100 nm. However, the results obtained by testing this structure revealed a problem. If the frame was fully closed, there are parts, such as the red area circled in the *Figure 18*, where the remaining liquid resist would not come out during the development process. This would lead to ruining of the whole structure. This problem was addressed by making a hole on one side of the wall, and removing the inner horizontal, vertical and diagonal lines of those layers. This is to say, the inside area was empty for these layers except for the surrounding wall so that the resist could run out from the hole during the developing process. The hole size was not chosen to be not too big and the position not too high in order not to influence the steadiness of the entire structure. In our experiments, the length of the hole was 10 µm, while the height was 1.2 µm which started from 2 µm above the ground extending to height of 3.2 µm. There was not too much difference if we adjusted the size of the hole slightly. *Figure 19* shows the formed structure (left) and the scheme of the hole (right).

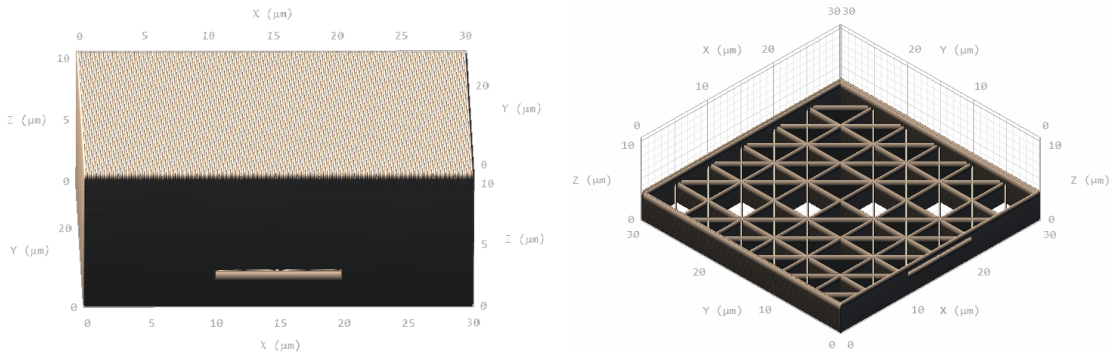

Figure 19. *The entire small structure including the side hole, seen from the hole side (left) and the structure in the layers of hole (right).*

After the stability of the small 30 µm × 30 µm × 10 µm box structure was affirmed, we adopted a straightforward approach that combined the small boxes together to constitute the entire structure. Although the height was still the same (10 µm), the width and length were thus larger (outside dimensions 180 µm and inners side 120 µm). It is notable that the holes were always placed to the inside edges, as the so called slope structures need to be added outside. *Figure 20* shows the frame design without external slopes.

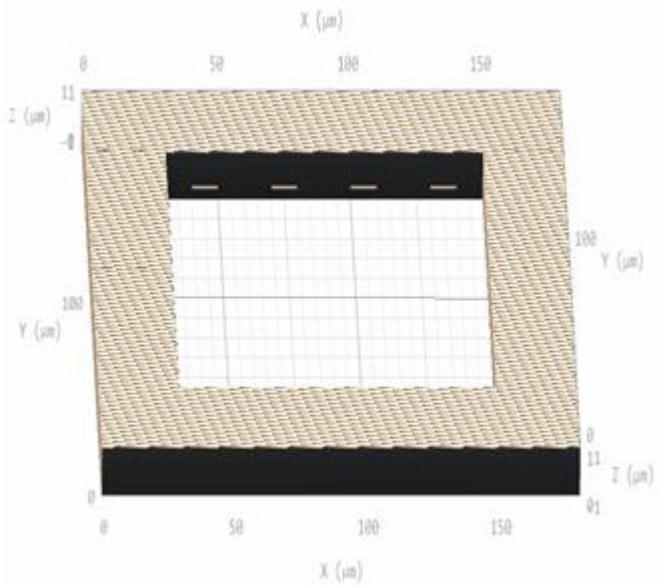

Figure20. *The whole box structure generated those smaller square elements showing in Figure 19.*

The slope structures for the outside edges of the box were fabricated in the following way: The width and the height of the slopes were both 10 µm, and their length was 180 µm. Again, a small hole was made on one side of the wall as well (see *Figure 21 (left)*). Here, the hole was made from 2 µm high above the surface to 3 µm and the width was

decreased to 5 µm. The inside frame of the slope was designed in the same way as small box, with a top view shown in *Figure 21 (right)*.

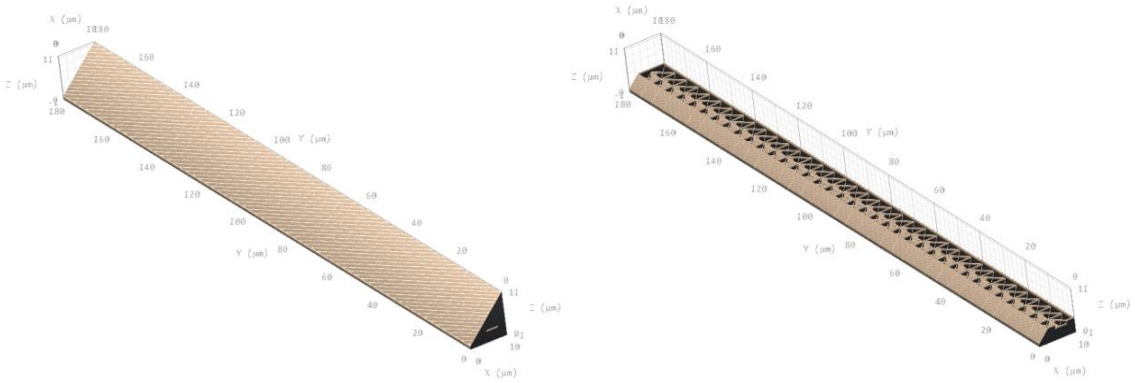

Figure 21. *The diagram of one slope (left) and the structure in the layers of hole (right).*

Finally, the whole structure was obtained by connecting them together via codes in Describe (see *Figure 22*).

Figure 22. *The final full structure, shown as a Matlab gwl-file.*

4.3 Dipping tests

Apart from the structure tests, several dipping experiments were also made after the box structures were fabricated successfully. However, for these dipping tests, the entire structure would not be coated with gold after the fabrication, but they were used in solution directly. The sample was dipped vertically into the solution to a depth of about 9 mm. Then the arm was raised slowly to withdraw the sample from the solution. A schematic of the dipping method is shown in *Figure 23*. (It can also be dipped with an

angle which is not be discussed in this research)

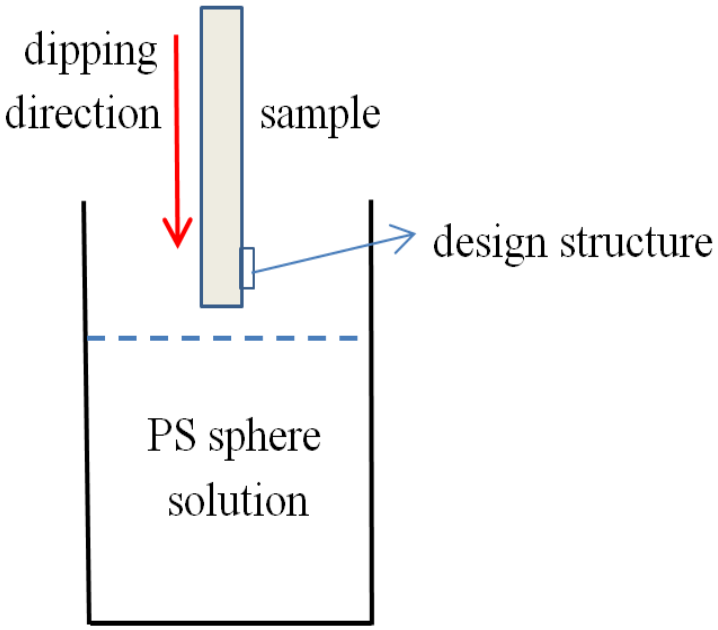

Figure 23. *Schematic of the dipping setup (vertically).*

The samples were held by the sample holder that located at the bottom of the dipping arm which the movement could be controlled by a software interface. And a PS nanospheres solution container was put on the stage where the samples could be submerged, see *Figure 24*. In addition, it has been studied that the withdrawal speed and the concentration of the solution are the main factors influencing the dipping results. [27] Therefore, here, the concentrations of the PS nanoparticle solutions used in the tests were 0.2 %, 1 % and 2 %, while the withdrawal speeds used were 0.01 mm/min and 0.02 mm/min. The original concentration of the solution was 10 % which was bought from Duke Scientific. [27] It was diluted with de-ionized water to the concentration we wanted. After the dipping process, the samples were coated with Au so that they could be imaged with SEM. Good dipping results were achieved only when the concentration was 1 % and the speed was 0.01 mm/min, shown in the next chapter.

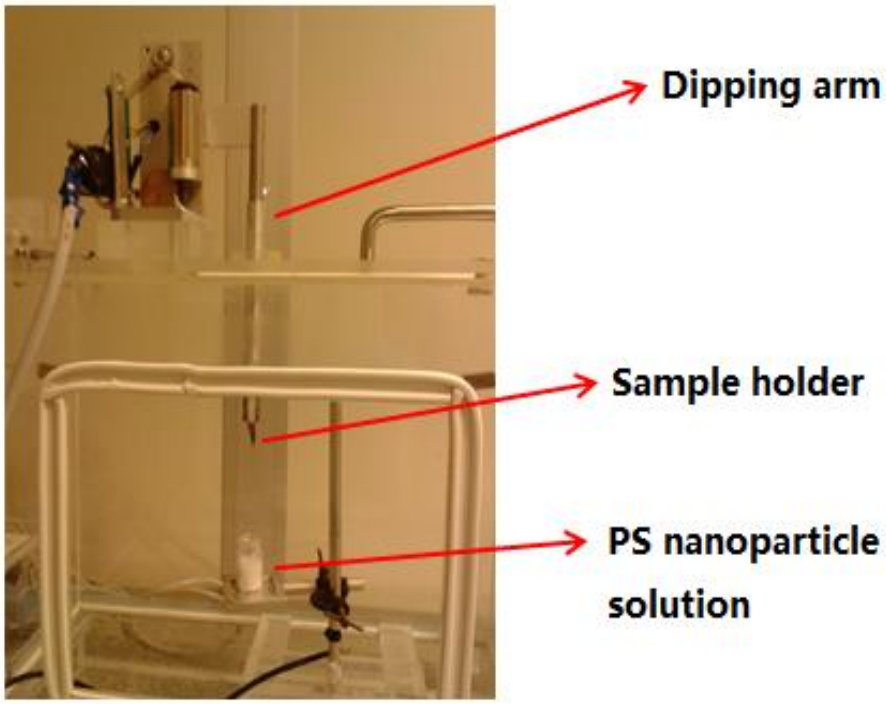

Figure 24. An image of the dipping instrument.

5 RESULTS AND DISCUSSION

This chapter will discuss the results and difficulties in the experiments. *Figure 25* illustrates some achieved results of the box fabrication, by imaging the structures with SEM. In practice, the measured dimensions (roughly 162 µm outer side and 107 µm inner side) of these structures are less than the values we set in the beginning (180 µm outer side and 120 µm inner side). In addition, the whole structure is bent, while only some of the box area is attached to the substrate, which can be seen more clearly in *Figure 25 (b)*. One of the reasons leading to this phenomenon may be because of the stresses in the structure. Additionally, another possible reason may be the changes in the refractive index from liquid to solid state of the resist during the fabrication process, which could influence the laser focus position. [39]

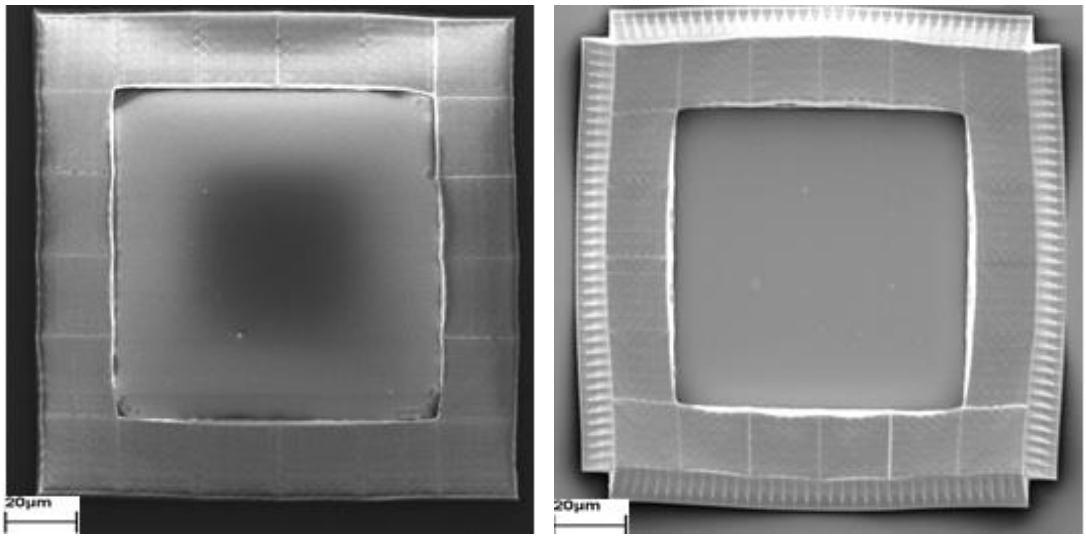

(a) (b)

Figure 25. *Images of the fabricated boxes results with SEM: (a) without slopes; (b) with slopes.*

The images after deposition of the PS colloidal crystal by dipping are depicted in *Figure 26*. Fortunately, although there are some problems, the results display that the box does make a difference during the dipping process, showing some benefits. One advantage is that there are no nanospheres on the surface of the structure but just inside the hollow

box and outside of the structure (see *Figure 26 (a)*). The PS colloidal crystal inside the box does still have domains defected by cracks, but the domain size is rather large with an average value is about 30 μm, as we can see in *Figure 26 (b)*. What's more, there is a clear multi-layer colloidal crystal structure formed during this process, which is shown in *Figure 27*.

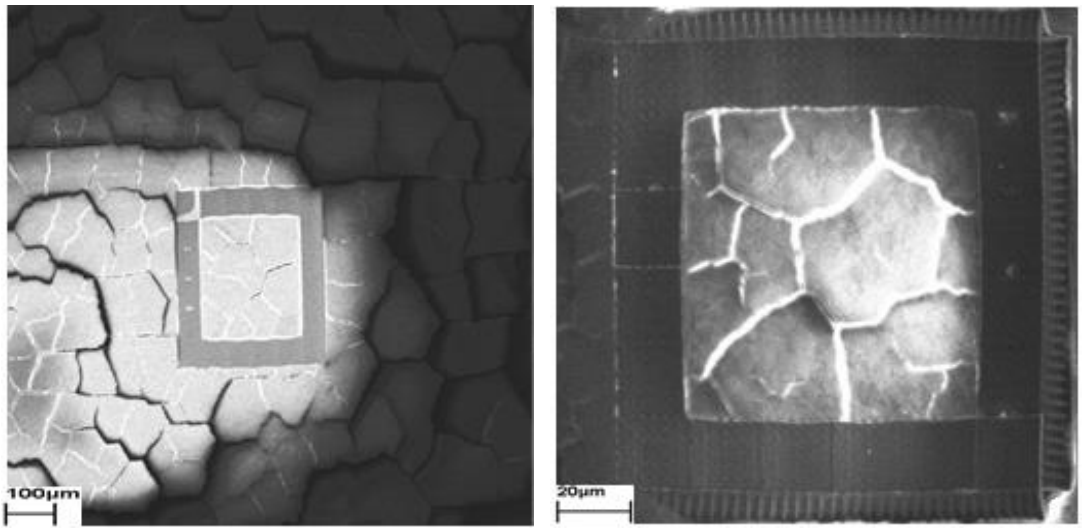

(a) (b)

Figure 26. *The image results after dipping process: (a) without slopes; (b) with slopes.*

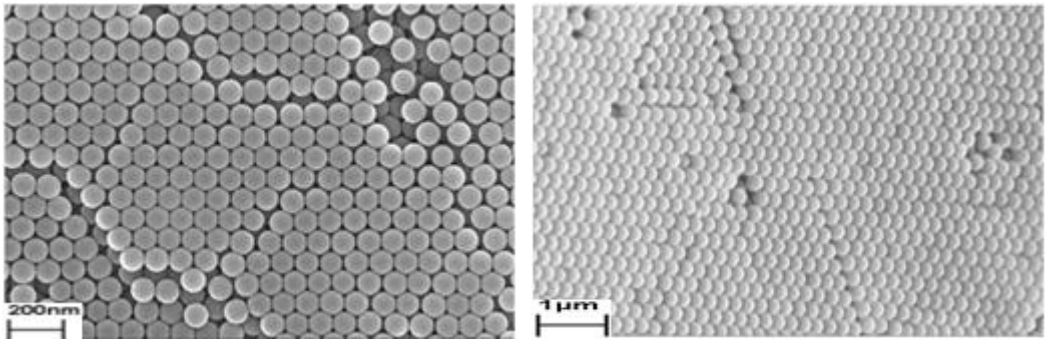

Figure 27. *Top view of colloidal structure (left) and side view of the structure (right).*

Nonetheless, the dipping results also display some problems which need to be addressed. First of all, as mentioned above, since there is only a small area where the box sticks to the substrate, it is much easier for the whole structure to detach from the glass during the dipping procedure. Secondly, nanospheres do not seem to order inside the empty area with a single domain, bringing about some cracks. However, the cracks seem to be either non-existent or much narrower at the contact with the box side walls. Furthermore, since the total structure is fabricated by combining small boxes together,

the surface is not totally smooth, and there are sometimes small holes on the connection part of some boxes (see *Figure 28*).

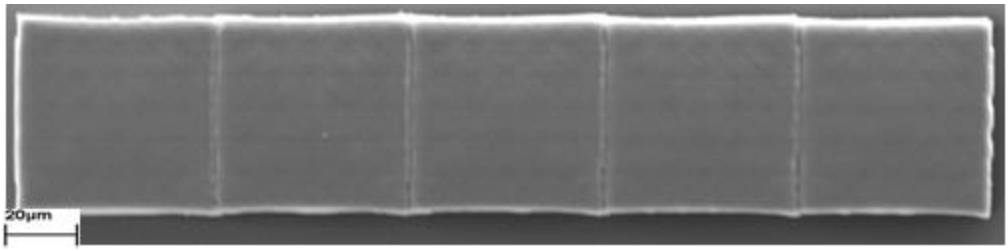

Figure 28. *The structure formed by connecting small boxes.*

We try to tackle these problems in the following tests. Among them, one improved result is achieved by extending the length of the boxes around the four corners, as seen in *Figure 29*. This approach allows a larger area to adhere on the glass substrate. With this method, the walls of the formed box become much straighter than in the results before. This may happen because the strain can be distributed more evenly, which is favorable for pulling the structure back to the substrate and balancing the total structure. However, there is still a clear shrinkage effect and detaching at the extension parts.

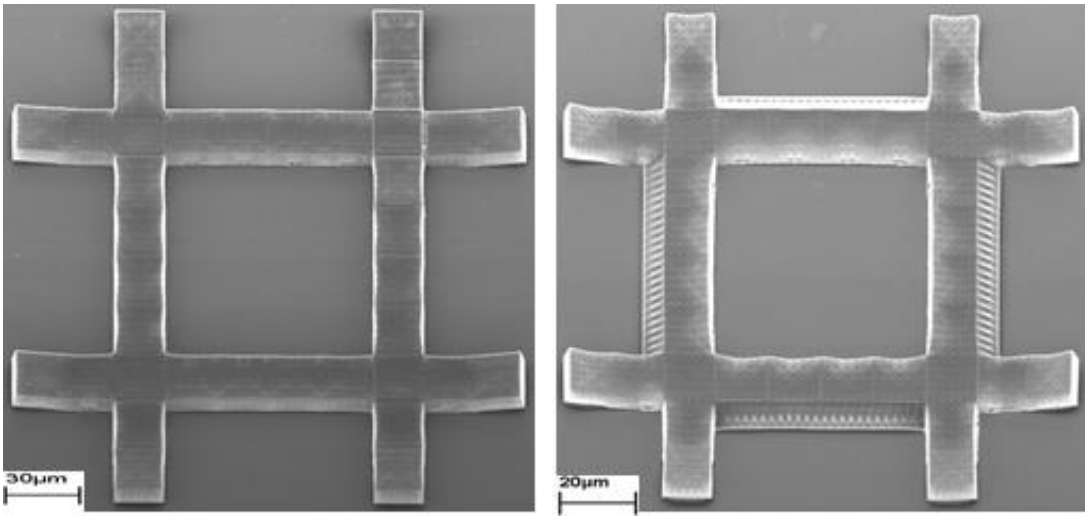

(a) (b)

Figure 29. *A test with structure where walls are extended further: without slopes (a); with slopes (b).*

Another improvement that copes with the smoothness problem is achieved by employing a long cuboid structure instead of connecting several small boxes together. Using the design of the longer structure is same as before, the only difference between these two structures is that the length for the cuboid increases to 150 μm. *Figure 30 (a)*

shows the image of the new structure. *Figure 30 (b)* displays the smoothness of the new structure. It is clear that in the new structure the walls are much straighter than in the old structure in *Figure 28*.

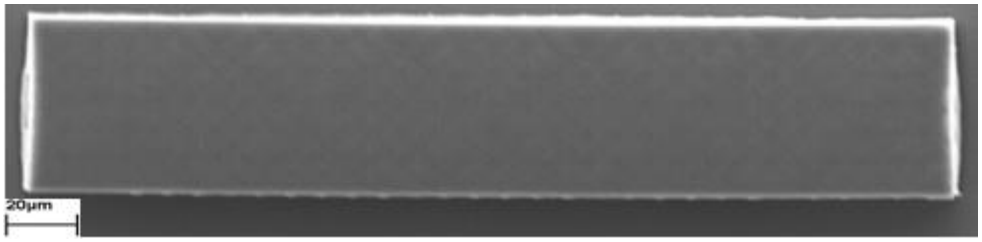

(a)

(b)

Figure 30. *SEM image of the new longer structure (a); Zoom-in of the surface (above structure) (b).*

In the structures discussed so far, the height of all the structures we measured is restricted to only around 10 µm. It is desired to increase the height to 20 µm if we want to get better dipping results. Therefore, we started to make fabrication of long cuboid structures but higher height. However, many problems appear when the height is just a little above 10 µm. In usual 3D-DLW, the depth of the structures can be limited due to the microscope lens working distance, and also because of the aberrations arising from the changed refractive-index upon polymerization. This can decrease the effective laser power when writing deep inside the photoresist. [26] Thus, the laser cannot be focused to the position correctly when the height is above some tens of micrometers, leading to big holes occurring on the surface (see *Figure 31*). We try to deal with this problem by

increasing the laser power, but that triggers another problem. The bottom part can "be boiled" when the laser power is too high, as seen in *Figure 32*.

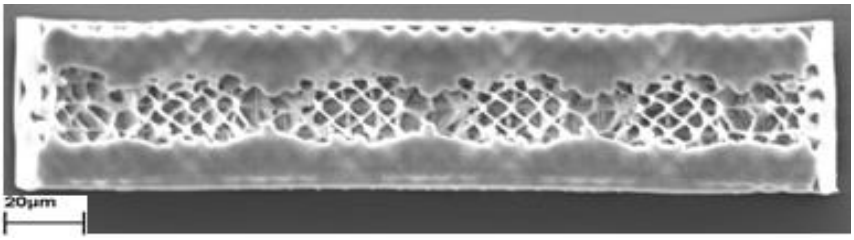

Figure 31. *An example when the height is 20 µm.*

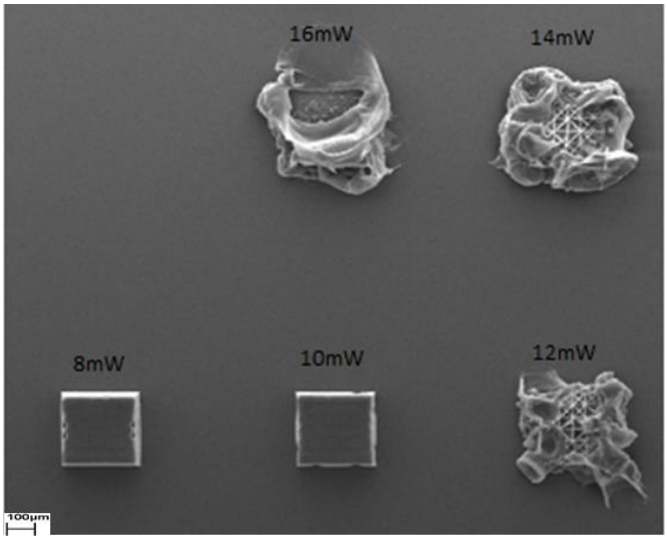

Figure 32. *Imaging results by testing different laser powers.*

Figure 32 reveals some results with different laser powers. The structure will be completely destroyed when the laser power is rather high (e.g. laser power value is 16 mW), whereas for the smaller value we can see small holes on the top side (e.g. the one laser power is 8 mW). This situation can be modified in some degree by setting different power values for different layers. Results by adjusting the power in a structure are presented in *Figure 33.*

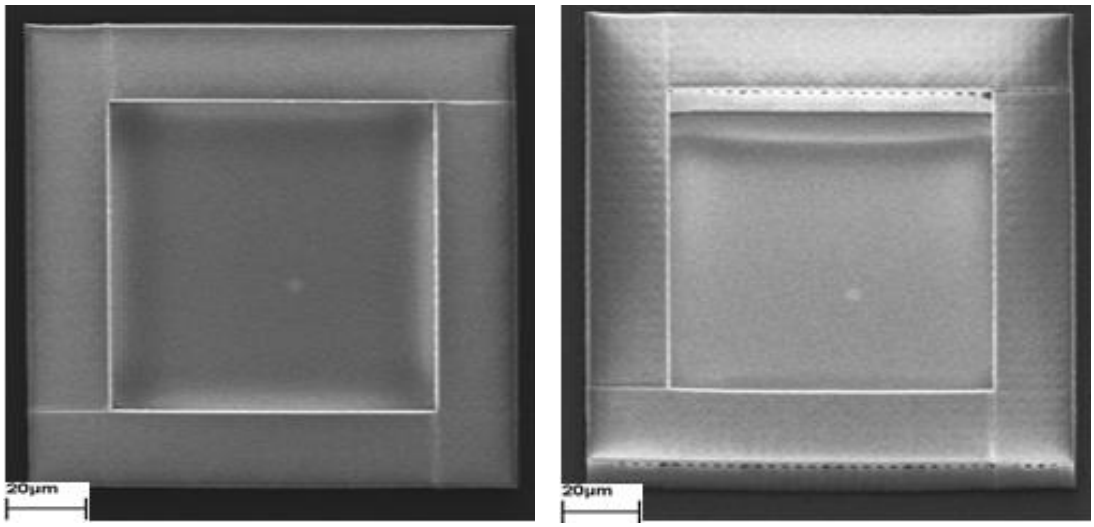

Figure 33. *Image of the results after setting different laser power for different layers: the top view (left) and side view (right).*

Here, the laser power is set at 8 mW from the ground to 2 μm height. Then the value changes to 9 mW till 3.6 μm, and it continues increasing to 10 mW from 3.6 μm to 19 μm. For the final 1 μm height, we use the value 14 mW. It shows much better results, without any holes on the top surface. However, there are still many holes on the side walls as shown in the figure. We do not yet know whether the holes will have a huge influence on the structure or not.

6 CONCLUSION

In conclusion, we have successfully fabricated the hollow box structure using the 3D lithography technique. Good results by dipping the obtained structures with nanospheres solutions were also achieved. However, several problems still exist. Although we managed to improve problems with deformation, some effects are still left. In addition, some cracks still appear in the formed colloidal crystal structure inside the box. The height of all structures could also be increased further.

REFERENCES

[1] *An Introduction to Lithography,* University of Warwick, Uk, 2004, Available: http://www.caiciss.co.uk/lithography.pdf.

[2] Babak Ziaie, Antonio Baldi, Massood Z. Atashbar, *Introduction to Micro-/Nanofabrication, Springer, (2010) 231-265.*

[3] Marc J. Madou, *Fundamentals of Microfabrication: The Science of Miniaturization, CRC Press, Second Edition, (2002) 1-2.*

[4] Michael Thiel and Martin Hermatschweiler, *Three-dimensional laser lithography, Optik & Photonik, 6 (2011) 36–39.*

[5] G. Cojoc, C. Liberale, P. Candeloro, F. Gentile, G. Das, F. De Angelis, E. Di Fabrizio, *Optical micro-structures fabricated on top of optical fibers by means of two-photon photopolymerization, Microelectronic Engineering, 87 (2010) 876–879.*

[6] Maria Farsari and Boris N.Chichkov, *Materials processing: Two-photon fabrication, Nature Photonics, 3 (2009) 450 – 452.*

[7] Attilio Marino, Gianni Ciofani, Carlo Filippeschi, Mario Pellegrino, Monica Pellegrini, Paolo Orsini, Massimo Pasqualetti, Virgilio Mattoli, Barbara Mazzolai, *Two-Photon Polymerization of Sub-micrometric Patterned Surfaces: Investigation of Cell-Substrate Interactions and Improved Differentiation of Neuron-like Cells, ACS Appl. Mater. Interfaces, 5 (2013) 13012–13021.*

[8] V.Schmidt, L.Kuna, V.Satzinger, G.Jakopic, G.Leising, *Two-photon 3D lithography: A Versatile Fabrication Method for Complex 3D Shapes and Optical Interconnects within the Scope of Innovative Industrial Applications, JLMN-Journal of Laser Micro/Nanoengineering, 2 (2007) 170-177.*

[9] F. Klein, B. Richter, T. Striebel, C. M. Franz, G. von Freymann, M. Wegener, M. Bastmeyer, *Two-component polymer scaffolds for controlled three-dimensional cell culture, Adv. Mater., 23 (2011) 1341-1345.*

[10] Shoji Maruo, Koji Ikuta, and Hayato Korogi, *Force-Controllable, Optical Driven Micromachines Fabricated by Single-Step Two-photon Microstereolithography, Journal of Microelectromechanical Systems, 12 (2003) 533–539.*

[11] Da Yang, Shalin J. Jhaveri and Christopher K Ober, *Three-Dimensional Microfabrication by Two-Photon Lithography, MRS Bulletin, 30 (2005) 976-982.*

[12] Hong-Bo Sun, Makoto Maeda, and Kenji Takada, James W. M. Chon and Min Gu, Satoshi Kawata, *Experimental investigation of single voxels for laser nanofabrication via two-photon photopolymerization. Appl. Phys. Lett., 83 (2003) 819.*

[13] Shuhui Wu, Jesper Serbin, Min Gu, *Two-photon polymerization for three-dimensional micro-fabrication, Journal of Photochemistry and Photobiology A: Chemistry, 181 (2006) 1–11.*

[14] Mohammed Al- Abaddi, Luigi Sasso, Maria Dimaki, Winnie E. Svendsen, *Fabrication of 3D nano/microelectrodes via two-photon-polymerization, Microelectronic Engineering, 98 (2012) 378-381.*

[15] M. Goeppert-Mayer, *Über Elementarakte mit zwei Quantensprüngen, Annals of Physics, 9 (1931) 273.*

[16] I. P´erez-Arjona, G.J. de Valc´arcel, and Eugenio Rold´an, *Two–photon absorption, Revista Mexicana de Fisica, 49 (2003) 91-100.*

[17] Semere Ghebru Bairu, *Ultrafast Dynamics and Two-Photon Absorption Properties of Chromophores at Interfaces,* PhD thesis, Department of Chemistry, Western Michigan University, 2013. Available: http://scholarworks.wmich.edu/cgi/viewcontent.cgi?article=1177&context=dissertations.

[18] Satoshi Kawata, Hong-Bo Sun, *Two-photon photopolymerization as a tool for making micro-devices, Applied Surface Science, 208-209 (2003) 153-158.*

[19] Hong-Bo Sun, Satoshi Kawata1, *Two-Photon Photopolymerization and 3D Lithographic Microfabrication, Advances in Polymer Science, 170 (2004) 169-273.*

[20] W. Kaiser, and C.G.B. Garrett, *Two-Photon Excitation in CaF_2: Eu^{2+}, Phys. Rev. Lett., 7 (1961) 229.*

[21] Satoru Shoji and Satoshi Kawata (eds.), *Nanofabrication Handbook, CRC Press, (2012) 229-249.*

[22] Daniel S. Correa, Leonardo De Boni, Adriano J. G. Otuka, Vinicius Tribuzi Cleber R. Mendonça and Ailton De Souza Gomes (Ed.), *Polymerization, InTech, (2012) 333-356.*

[23] Theodor Asavei, Timo A. Nieminen, Norman R. Heckenberg and Halina Rubinsztein-Dunlop, *Fabrication of micro-structures for optically driven micromachines using two-photon photopolymerization of UV curing resins, Journal of Optics A, 11(2009) 7.*

[24] Shoji Maruo, Osamu Nakamura, and Satoshi Kawata, *Three-dimensional microfabrication with two-photon-absorbed photopolymerization, Optics Letters, 22 (1997) 132-134.*

[25] *NanoScribe true 3D Laser Lithography,* Available: http://www.nanoprecision-3d.com/pics/Products/Version2.2.pdf.

[26] Tiemo Bückmann, Nicolas Stenger, Muamer Kadic, Johannes Kaschke, Andreas Frölich, Tobias Kennerknecht, Christoph Eberl, Michael Thiel, and Martin Wegener, *Tailored 3D Mechanical Metamaterials Made by Dip-in Direct-Laser-Writing Optical Lithography, Adv. Mater., 24 (2012) 2710-2714.*

[27] Tero Isotalo, *Periodic nanostructures for thermal engineering applications*, PhD thesis, Department of Physics, University of Jyväskylä, February 2014. Available: http://www.jyu.fi/static/fysiikka/vaitoskirjat/2014/Isotalo-Tero-2014.pdf.

[28] Tero J. Isotalo, Yao-Lan Tian, Mikko P. Konttinen, Ilari J. Maasilta, *Statistical Characterization of Self-Assembled Colloidal Crystals by Single-Step Vertical Deposition, Colloids and Surfaces A: Physicochem. Eng. Aspects, 443 (2014) 164-170.*

[29] *NanoScribe Photonic Professional User Manual,* Nanoscribe GmbH, Germany, 2013.

[30] *Data sheet PHOTONIC PROFESSIONAL GT,* Available: http://www.nanoscribe.de/files/9613/8737/0062/DataSheet_Photonic_Professional_GT.pdf.

[31] *Data sheet IP-PHOTORESISTS,* Available: http://www.nanoscribe.de/files/1213/8251/8144/IP-Resist_IP-Dip.pdf.

[32] *NanoScribe Applications,* Avaliable: http://www.nanoscribe.de/en/applications/.

[33] Lina Yang, Nuo Yang and Baowen Li, *Reduction of Thermal Conductivity by Nanoscale 3D Phononic Crystal*, *Scientific Report, 3 (2013) 1143.*

[34] Mark Holm Olsen, *Two-photon polymerization of immune cell scaffolds*, PhD thesis, DTU Nanotech, Department of Micro- and Nanotechnology, Technical University of Denmark, September 2013. Available: http://orbit.dtu.dk/ws/files/82890420/prod11387460099286.Mark_Olsen_PhD_1.pdf.

[35] Christopher N. LaFratta, John T. Fourkas, Tommaso Baldacchini, and Richard A. Farrer, *Multiphoton Fabrication*, *Journal: ChemInform , 38 (2007) 6238-6258.*

[36] Hong-Bo Sun, Kenji Takada, Moon-Soo Kim and Kwang-Sup Lee, Satoshi Kawata, *Scaling laws of voxels in two-photon photopolymerization nanofabrication*, *Appl. Phys. Lett., 83 (2003) 1104-1106.*

[37] Thomas F. Wuhrmann, *Design, Fabrication and Characterization of Ferromagnetic Artificial Bacterial Flagella*, Master thesis, Institute of Robotics and Intelligent Systems, Swiss Federal Institute of Technology Zurich (ETH), 2011. Available: http://e-collection.library.ethz.ch/eserv/eth:5014/eth-5014-01.pdf.

[38] Zipfel, W. R., Williams, R. M. & Webb, W. W, *Nonlinear magic: multiphoton microscopy in the biosciences*, *Nature biotechnology, 21 (2003) 1369–77.*

[39] Kwang-Sup Lee, Ran Hee Kim, Dong-Yol Yang, Sang Hu Park, *Advances in 3D nano/microfabrication using two-photon initiated polymerization*, *Prog. Polym. Sci., 33 (2008) 631-681.*

APPENDIX A

An example of the Matlab code of the box which shown in *Figure 17* left:

```
function f=backside_3
Filename='backside_3';
Line_Space=0.2; %200µm
Z1max=9.6; %length in z-axis
z0=0:Line_Space:Z1max
Y11_1=30; %along y-axis the length is 30µm
for mm=1:length(z0)
  if 10>=mm % from 0-2µm, first draw outside two walls
% the first wall (most outside)
    line_start=[0,0,z0(mm)];
    line_stop=[30,0,z0(mm)];
          dlmwrite(Filename,line_start,'-append','delimiter',' ');
          dlmwrite(Filename,line_stop,'-append','delimiter',' ');
          dlmwrite(Filename,'write','-append','delimiter','');
    line_start=[30,0,z0(mm)];
    line_stop=[30,30,z0(mm)];
          dlmwrite(Filename,line_start,'-append','delimiter',' ');
          dlmwrite(Filename,line_stop,'-append','delimiter',' ');
          dlmwrite(Filename,'write','-append','delimiter','');
    line_start=[30,30,z0(mm)];
    line_stop=[0,30,z0(mm)];
          dlmwrite(Filename,line_start,'-append','delimiter',' ');
          dlmwrite(Filename,line_stop,'-append','delimiter',' ');
          dlmwrite(Filename,'write','-append','delimiter','');
    line_start=[0,30,z0(mm)];
    line_stop=[0,0,z0(mm)];
          dlmwrite(Filename,line_start,'-append','delimiter',' ');
          dlmwrite(Filename,line_stop,'-append','delimiter',' ');
          dlmwrite(Filename,'write','-append','delimiter','');
% the second wall
    line_start=[0.2,0.2,z0(mm)];
    line_stop=[30-0.2,0.2,z0(mm)];
          dlmwrite(Filename,line_start,'-append','delimiter',' ');
          dlmwrite(Filename,line_stop,'-append','delimiter',' ');
          dlmwrite(Filename,'write','-append','delimiter','');
    line_start=[30-0.2,0.2,z0(mm)];
    line_stop=[30-0.2,30-0.2,z0(mm)];
          dlmwrite(Filename,line_start,'-append','delimiter',' ');
          dlmwrite(Filename,line_stop,'-append','delimiter',' ');
          dlmwrite(Filename,'write','-append','delimiter','');
    line_start=[30-0.2,30-0.2,z0(mm)];
    line_stop=[0.2,30-0.2,z0(mm)];
          dlmwrite(Filename,line_start,'-append','delimiter',' ');
          dlmwrite(Filename,line_stop,'-append','delimiter',' ');
          dlmwrite(Filename,'write','-append','delimiter','');
    line_start=[0.2,30-0.2,z0(mm)];
    line_stop=[0.2,0.2,z0(mm)];
          dlmwrite(Filename,line_start,'-append','delimiter',' ');
```

```
          dlmwrite(Filename,line_stop,'-append','delimiter',' ');
          dlmwrite(Filename,'write','-append','delimiter','');
%start drawing lateral lines inside with distance of each line is 5µm
for Y11=5:Line_Space*25:Y11_1-5
        a=0;
        t=0;
        for i=1:length(Y11);
            t=t+a;
            if t==0
                  Line_Start=[0,Y11(i),z0(mm)];
                  Line_Stop=[30,Y11(i),z0(mm)];
                  a=1;
            else
                  Line_Start=[30,Y11(i),z0(mm)];
                  Line_Stop=[0,Y11(i),z0(mm)];
                  a=-1;
            end
              dlmwrite(Filename,Line_Start,'-append','delimiter',' ');
              dlmwrite(Filename,Line_Stop,'-append','delimiter',' ');
              dlmwrite(Filename,'write','-append','delimiter','');
        end
end
%start drawing vertical lines inside with distance of each line is 5µm
for X11=5:Line_Space*25:25
        a=0;
        t=0;

        for i11=1:length(Y11);
            t=t+a;
            if t==0
                  Line_Start=[X11(i11),0,z0(mm)];
                  Line_Stop=[X11(i11),30,z0(mm)];
                  a=1;
            else
                  Line_Start=[X11(i11),30,z0(mm)];
                  Line_Stop=[X11(i11),0,z0(mm)];
                  a=-1;
            end
               dlmwrite(Filename,Line_Start,'-append','delimiter','');
               dlmwrite(Filename,Line_Stop,'-append','delimiter',' ');
               dlmwrite(Filename,'write','-append','delimiter','');
        end
end
% start drawing intersection lines inside
     Y1=5:Line_Space*25:Y11_1-5
         for i_1=1:length(Y1)
          Line_Start_1=[Y1(i_1),0,z0(mm)];
          Line_Stop_1=[0,Y1(i_1),z0(mm)];
            dlmwrite(Filename,Line_Start_1,'-append','delimiter',' ');
            dlmwrite(Filename,Line_Stop_1,'-append','delimiter',' ');
             dlmwrite(Filename,'write','-append','delimiter','');
         end
         for i_1=1:length(Y1)
           Line_Start1_1=[30-Y1(i_1),30,z0(mm)];
           Line_Stop1_1=[30,30-Y1(i_1),z0(mm)];
            dlmwrite(Filename,Line_Start1_1,'-append','delimiter','');
            dlmwrite(Filename,Line_Stop1_1,'-append','delimiter',' ');
```

```
            dlmwrite(Filename,'write','-append','delimiter','');
        end
        for i_1=1:length(Y1)
          Line_Start_12=[30-Y1(i_1),0,z0(mm)];
          Line_Stop_12=[30,Y1(i_1),z0(mm)];
           dlmwrite(Filename,Line_Start_12,'-append','delimiter','');
           dlmwrite(Filename,Line_Stop_12,'-append','delimiter',' ');
           dlmwrite(Filename,'write','-append','delimiter','');
        end
        for i_1=1:length(Y1)
          Line_Start1_12=[0,30-Y1(i_1),z0(mm)];
          Line_Stop1_12=[Y1(i_1),30,z0(mm)];
          dlmwrite(Filename,Line_Start1_12,'-append','delimiter','');
          dlmwrite(Filename,Line_Stop1_12,'-append','delimiter',' ');
          dlmwrite(Filename,'write','-append','delimiter','');
        end
   end
% start drawing the layers with holes (2-3.2µm)
  if (16>mm)&&(mm>10)
% the first wall (most outside)
          Line_start=[0,0,z0(mm)];
          Line_stop=[10,0,z0(mm)];
              dlmwrite(Filename,Line_start,'-append','delimiter',' ');
              dlmwrite(Filename,Line_stop,'-append','delimiter',' ');
              dlmwrite(Filename,'write','-append','delimiter','');
          Line_start=[20,0,z0(mm)];
          Line_stop=[30,0,z0(mm)];
              dlmwrite(Filename,Line_start,'-append','delimiter',' ');
              dlmwrite(Filename,Line_stop,'-append','delimiter',' ');
              dlmwrite(Filename,'write','-append','delimiter','');
          Line_start=[30,0,z0(mm)];
          Line_stop=[30,30,z0(mm)];
              dlmwrite(Filename,Line_start,'-append','delimiter',' ');
              dlmwrite(Filename,Line_stop,'-append','delimiter',' ');
              dlmwrite(Filename,'write','-append','delimiter','');
          Line_start=[30,30,z0(mm)];
          Line_stop=[0,30,z0(mm)];
              dlmwrite(Filename,Line_start,'-append','delimiter',' ');
              dlmwrite(Filename,Line_stop,'-append','delimiter',' ');
              dlmwrite(Filename,'write','-append','delimiter','');
          Line_start=[0,30,z0(mm)];
          Line_stop=[0,0,z0(mm)];
              dlmwrite(Filename,Line_start,'-append','delimiter',' ');
              dlmwrite(Filename,Line_stop,'-append','delimiter',' ');
              dlmwrite(Filename,'write','-append','delimiter','');
% the second wall
          Line_start=[0.2,0.2,z0(mm)];
          Line_stop=[10,0.2,z0(mm)];
              dlmwrite(Filename,Line_start,'-append','delimiter',' ');
              dlmwrite(Filename,Line_stop,'-append','delimiter',' ');
              dlmwrite(Filename,'write','-append','delimiter','');
          Line_start=[20,0.2,z0(mm)];
          Line_stop=[30-0.2,0.2,z0(mm)];
              dlmwrite(Filename,Line_start,'-append','delimiter',' ');
              dlmwrite(Filename,Line_stop,'-append','delimiter',' ');
              dlmwrite(Filename,'write','-append','delimiter','');
          Line_start=[30-0.2,0.2,z0(mm)];
```

```
            Line_stop=[30-0.2,30-0.2,z0(mm)];
                dlmwrite(Filename,Line_start,'-append','delimiter',' ');
                dlmwrite(Filename,Line_stop,'-append','delimiter',' ');
                dlmwrite(Filename,'write','-append','delimiter','');
            Line_start=[30-0.2,30-0.2,z0(mm)];
            Line_stop=[0.2,30-0.2,z0(mm)];
                dlmwrite(Filename,Line_start,'-append','delimiter',' ');
                dlmwrite(Filename,Line_stop,'-append','delimiter',' ');
                dlmwrite(Filename,'write','-append','delimiter','');
            Line_start=[0.2,30-0.2,z0(mm)];
            Line_stop=[0.2,0.2,z0(mm)];
                dlmwrite(Filename,Line_start,'-append','delimiter',' ');
                dlmwrite(Filename,Line_stop,'-append','delimiter',' ');
                dlmwrite(Filename,'write','-append','delimiter','');
        end

% from the height from 3.2µm to 9.6µm, use the same code in the height
from 0 to 2µm (just change to if mm>16 in the beginning)

% the left two top layers with the distance in lateral direction is
100µm
for Z2=9.8:0.2:10
for X2=0:0.1:30
    t=0;
    a=0;
    for x2=1:length(X2)
        t=t+a;
        if t==0
             Line_Start=[X2(x2),0,Z2];
             Line_Stop=[X2(x2),30,Z2];
             a=1;
            else
             Line_Start=[X2(x2),30,Z2];
             Line_Stop=[X2(x2),0,Z2];
             a=-1;
            end
              dlmwrite(Filename,Line_Start,'-append','delimiter',' ');
              dlmwrite(Filename,Line_Stop,'-append','delimiter',' ');
              dlmwrite(Filename,'write','-append','delimiter','');
    end
end
end
end
```

APPENDIX B

The example of the code in Describe:

```
PiezoScanMode
ContinuousMode
ConnectPointsOn
PerfectShapeIntermediate
TimestampOn

TiltCorrectionOn
Measuretilt 3

InvertZAxis 0
XOffset 0
YOffset 0
ZOffset 0
FindInterfaceAt 0.2

LaserPower 40
SettlingTime 200

PowerScaling 1
FindInterfaceAt 0.2
Include backside_3.gwl
Write

% if we want two boxes together in lateral direction
% AddXOffset 30
% Include backside_3.gwl
% Write
% if we want two boxes together in vertical direction
% AddYOffset 30
% Include backside_3.gwl
% Write
```